

Active motion of tangentially-driven polymers in periodic array of obstacles

Mohammad Fazelzadeh,¹ Ehsan Irani,² Zahra Mokhtari,³ and Sara Jabbari-Farouji ^{*1}

¹*Institute of Physics, University of Amsterdam, Amsterdam, The Netherlands*

²*Institute for Theoretical Physics, Georg-August University of Göttingen,
Friedrich-Hund Platz 1, 37077 Göttingen, Germany*

³*Department of Mathematics and Computer Science,
Freie Universität Berlin, Arnimallee 6, 14195 Berlin, Germany*

(Dated: October 3, 2023)

We computationally investigate the active transport of tangentially-driven polymers with varying degrees of flexibility and activity in two-dimensional square lattices of obstacles. Tight periodic confinement induces notable conformational changes and distinct modes of transport for flexible and stiff active filaments. It leads to localization and caging of flexible polymers inside the inter-obstacle pores, while promoting more elongated conformations and enhanced diffusion for stiff polymers at low to moderate activity levels. The migration of flexible active polymers occurs via hopping events, where they unfold to move from one cage to another. In contrast, stiff chains travel mainly in straight paths within inter-obstacle channels, while occasionally changing their direction of motion. Both the duration of caging and persistent directed migration within the channels decrease with increasing the activity level. As a consequence, at high active forces polymers overcome confinement effects and transport within inter-obstacle pores as swiftly as those in free space. We explain the center of mass dynamics of semiflexible polymers in terms of active force and obstacle packing fraction by developing an approximate analytical theory.

I. INTRODUCTION

Understanding the dynamics of active particles within heterogeneous media, subjected to intricate geometric constraints, has become an increasingly important research focus [1]. This elevated interest arises due to the omnipresence of porous media in both natural settings, such as gels, tissues, and soils, and man-designed devices like array of micro-pillars in bio-technological applications. Gaining such insight is of relevance from both fundamental and applied perspectives. From a fundamental viewpoint, we are interested in understanding the impact of the heterogeneity of environments on the stochastic transport of active particles within complex media. From a practical standpoint, it helps us to unveil the movement and search strategies employed by living organisms in real-world environments. Furthermore, the knowledge acquired can be harnessed to pioneer innovative technological applications for controlling the motion of active agents within complex media. For example, smart self-propelled carriers can be used for cargo or drug delivery in heterogeneous media or contamination removal in porous soil.

In the last decade, both experimental and theoretical research efforts [1–17] have been directed at understanding the motion of active particles in heterogeneous porous media. The majority of studies so far have focused on the migration of active particles in disordered media [1–9] as most of movement environments for active particles in the nature are disordered. However, patterned structures with periodic lattices are also found in the nature, for instance in antibiofouling surfaces such as cicada wings [18] and shark skins [19]. Moreover, a first approach to control the dynamics of active agents for technological applications relies on designing ordered heterogeneous media

by placing obstacles on a substrate in periodic arrangements [17, 20].

Research in this direction includes studies of the motion of active particles and bacteria [12–17] in periodic array of obstacles. These studies revealed that the periodic arrangement can enhance the persistent motion of active particles at high enough activity levels [15] and more generally affect the transport efficiency of active particles, depending on the size of active particles and the nature of their interactions with the structured medium. While the previous studies of active particles in periodic array of obstacles focused on rigid or spherical swimmers, not much is known about the motion of flexible elongated self-propelled particles, such as active filaments in periodic environments. As a first step in this direction, we investigate the motion of active polymers in a square lattice of obstacles. We note that although there have been several studies of active polymers in disordered porous media [9, 10], to our knowledge, effects of a periodic arrangement of obstacles on conformation and dynamics of active filaments remain unexplored. We choose to focus on tangentially-driven active polymers in a 2D square lattice which are relevant for experiments of *T. Tubifex* worms or E-coli bacteria in ordered two dimensional array of pillars [17, 20].

The key question that we address is under what conditions and how conformation and dynamics of active polymers are affected by the presence of ordered array of obstacles. To this end, we study the conformational and dynamical features of polymers while varying their degree of flexibility, activity level and the porosity of the ordered medium via changing packing fraction of obstacles. We find that the effect of periodic confinement becomes significant at high obstacle packing, where the pore size becomes smaller than the gyration radius of flexible poly-

mers or persistence length of semiflexible polymers.

Under tight confinement, flexible active polymers exhibit shrunken conformations which are predominantly caged in interobstacle pores and their transport occurs via rare events where they unfold and hop to an adjacent cage. In contrast, tight periodic confinement constrains active filaments to travel in straight paths inside the periodic channels while occasionally bend and change their directions. These two distinct modes of transport for flexible and stiff polymer lead to different trends for the long-time diffusion of active polymers at low to moderate activity levels. At low activities, tight periodic confinement decreases the long-time diffusion of flexible polymers, whereas for very stiff polymers it leads to enhancement of the long-time diffusion. Remarkably, for all the cases, at high activity levels, polymers exhibit a similar dynamics to those in free space, hence overcoming the effects imposed by tight geometrical constraints.

The remainder of this article is organized as follows. First, we introduce our simulation setup and the relevant set of dimensionless group of parameters. In section III, we investigate the effects of periodic arrays of obstacles on the conformation of active polymers under different situations. In section IV, we discuss distinct modes of transport for flexible and stiff polymers under strong confinement. We characterize the statistical features of caging events for flexible polymers and the channel switching events for stiff ones. In section V, we examine the effect of periodic confinement on dynamical properties of active polymers of varying degrees of activity and flexibility. Additionally, we propose analytical approach to rationalize the dynamics of the center of the mass of active chains under periodic confinement using suitable approximations. Finally, we summarize our most important findings and our concluding remarks in section VI.

II. SIMULATIONS DETAILS

A. Simulation model for active polymers and their interactions with obstacles

In order to study the motion of semiflexible active polymers in ordered heterogeneous media, we implement the tangentially-driven polymer model [21] in a 2D square lattice of circular obstacles, see Fig. 1. In experiments [17, 20], 2D projection of 3D active filaments around cylindrical pillars are observed, which implies that polymer can cross itself. To mimic this situation, we discard excluded volume interactions between monomers and we consider a phantom active polymer model of N monomers. The motion of each monomer is governed by the overdamped Langevin dynamics and is given by

$$\gamma \dot{\mathbf{r}}_i = - \sum_j \nabla_{\mathbf{r}_i} U + \mathbf{f}_i^a + \mathbf{f}_i^r, \quad (1)$$

where \mathbf{r}_i is the position of the i th monomer, the dot denotes the derivative with respect to time and γ is the friction coefficient between the bead and its surrounding medium.

The potential energy U of each monomer includes three different contributions. The first one is the harmonic spring potential $U_{\text{harmonic}}(r) = (k_s/2)(r - \ell)^2$, with equilibrium length ℓ and spring stiffness k_s between adjacent monomers. The Second part is the bending potential between each two neighbouring bonds $U_{\text{bend}}(\theta_i) = \kappa(1 - \cos\theta_i)$, where θ_i denotes the angle between two consequent bonds intersecting at bead i defined as $\theta_i = \cos^{-1}(\hat{\mathbf{t}}_{i,i+1} \cdot \hat{\mathbf{t}}_{i-1,i})$ with $\hat{\mathbf{t}}_{i,i+1} = \mathbf{r}_{i,i+1}/|\mathbf{r}_{i,i+1}|$ and $\mathbf{r}_{i,i+1} = \mathbf{r}_{i+1} - \mathbf{r}_i$. Here, κ is the bending stiffness and determines the intrinsic degree of flexibility of a polymer. Finally, the third contribution accounts for the excluded volume interactions between each bead and its surrounding obstacles. They are modelled by the short-ranged Weeks-Chandler-Andersen (WCA) potential [22] $U_{\text{excl}}(r) = 4\epsilon \left[\left(\frac{\sigma/2+r_o}{r} \right)^{12} - \left(\frac{\sigma/2+r_o}{r} \right)^6 + \frac{1}{4} \right]$ for $r < r_c = 2^{1/6}(\sigma/2 + r_o)$, where ϵ is the strength of the potential and has unit of energy, σ is the diameter of the beads and r_o is the radius of obstacles. The WCA potential is zero for interaction distances larger than the cutoff length r_c .

The active force on each bead, except for the end monomers, is given by: $\mathbf{f}_i^a = \frac{f^a}{2\ell}(\mathbf{r}_{i-1,i} + \mathbf{r}_{i,i+1})$. The active force on the tail monomer is given by $\mathbf{f}_1^a = \frac{f^a}{2\ell}\mathbf{r}_{1,2}$ and for the head monomer is $\mathbf{f}_N^a = \frac{f^a}{2\ell}\mathbf{r}_{N-1,N}$. For this model, the total active force on each polymer is proportional to its end-to-end vector $\mathbf{F}^a(t) = f^a \mathbf{R}_e(t)/\ell$. The random force is chosen as a white noise of zero mean and has the correlation $\langle \mathbf{f}_i^r(t) \cdot \mathbf{f}_j^r(t') \rangle = 4D_0\gamma^2\delta_{ij}\delta(t-t')$. To keep our formulation general, we do not associate random force necessarily with thermal fluctuations, but it can also be of biological origin. The persistence length of a 2D passive ideal polymer in free space can be determined in terms of its bending stiffness and the strength of random force correlation as $\ell_p^0 = 2\kappa\sigma/D_0\gamma$ [23].

We use a fixed number of N_o obstacles arranged in a square lattice in an $L \times L$ simulation box with periodic boundary conditions. To change the degree of confinement, we vary the packing fraction of the medium defined as the fraction of the surface occupied by the obstacles to the total area of the box $\phi = N_o\pi r_o^2/L^2$. The width of horizontal/vertical channels ξ is given by the free space between two neighbouring obstacles as shown in Fig. 1 and it is obtained as $\xi = r_o(\sqrt{\pi/\phi} - 2)$. We also define the approximate cage diameter (pore size) as $d_{\text{cage}} = r_o(\sqrt{2\pi/\phi} - 2)$, see Fig. 1. For flexible polymers, we can use the ratio of mean polymer size to the cage diameter as a measure of confinement strength, whereas for semiflexible polymers with $\kappa \gg 1$, the ratio of the persistence length to the channel width ℓ_p^0/ξ provides a

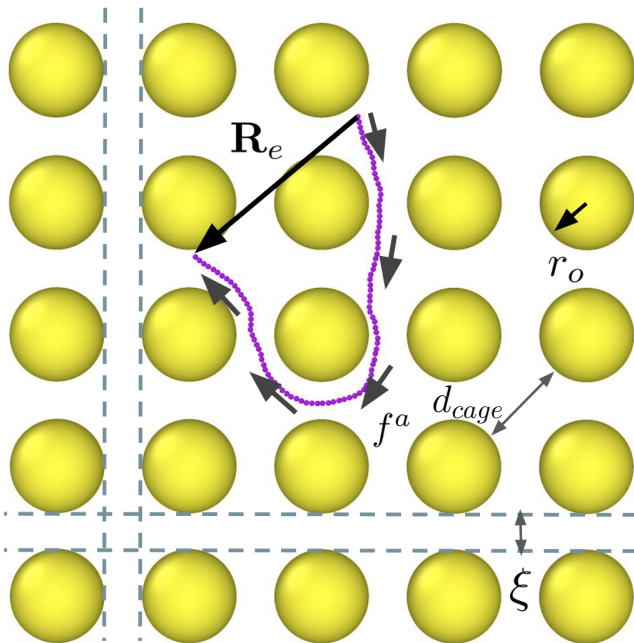


FIG. 1. Schematic of the active tangentially-driven polymer in the ordered array of obstacles, showing the end-to-end vector $\mathbf{R}_e = \mathbf{r}_N - \mathbf{r}_1$, the radius of obstacles r_o , the pore size d_{cage} and the horizontal/vertical channels of width ξ .

good measure of confinement degree.

B. Simulation parameters

We choose $l_u = \sigma$, $E_u = \epsilon$ and $\tau_u = \gamma\sigma^2/\epsilon$ with $\gamma = 1$ as the units of length, energy and time. From here on, we express quantities in dimensionless units. We subsequently fix $\ell = 1$, $r_o = 8.7$ and the diffusion coefficient $D_0 = 1$. The spring constants are chosen very stiff $k_s \gg f^a/\ell$, to ensure that the mean bond-length and polymer contour length remain almost constant during simulations. We focus on the chain length $N = 100$ and investigate the effects of periodic confinement on the conformational and the dynamical properties of active polymers of varying activity strengths $0.001 \leq f^a \leq 10$ and bending rigidity values $\kappa \in \{1, 10, 100\} \epsilon$. We examine the conformation and dynamics of active polymers under moderate ($\phi = 0.2$) and strong ($\phi = 0.6$) confinement leading to channel widths $\xi \in \{17, 2.5\} \sigma$, respectively and compare them with those of active polymers in free space ($\phi = 0.0$). To analyze the effects of periodic arrays of obstacles on conformation and dynamics of the polymers, we studied ensemble-averaged conformational and dynamical properties of active filaments, where $\langle \dots \rangle$ indicates ensemble average over 120 independent simulation runs carried over a time span at least 5 times larger than the relaxation time of the end-to-end vector, for details please see supplemental material (SM [24], section I).

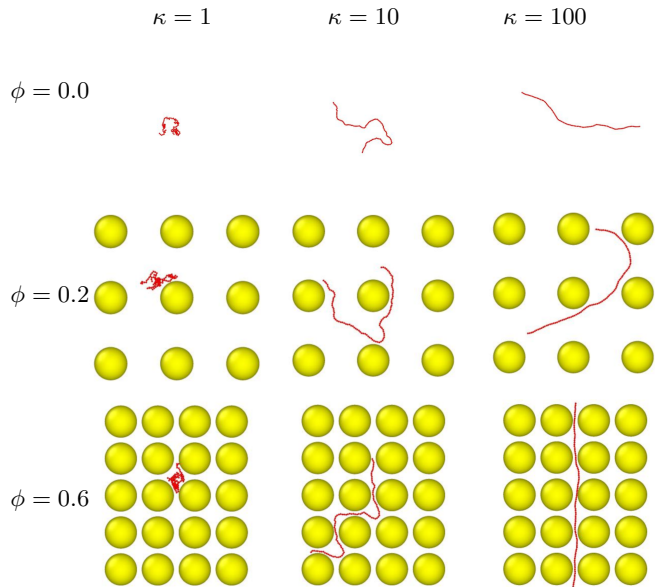


FIG. 2. Snapshots of an active chain with $f^a = 1$ in various combination of ϕ and κ . See videos S1-S9 at SM for temporal evolution of an active polymer conformation moving through the obstacles.

III. CONFORMATIONAL PROPERTIES

We begin by visually inspecting the effect of confinement degree on chain conformation. In Fig. 2, we present snapshots of active polymers with $f^a = 1.0$ for various combinations of bending stiffness and packing fraction values. The overall trend that we observe for flexible chains ($\kappa = 1$) is that by increasing the degree of confinement, at the highest studied packing fraction ($\phi = 0.6$) the polymers become localized in the cages of their adjacent obstacles for the majority of time. As a result, their mean size shrinks. In contrast, for stiffer chains with $\kappa \geq 10$, under strong confinement at $\phi = 0.6$, the chains conformation becomes more extended and anisotropic as the persistence length becomes larger than the channel width.

A. End-to-end distance

To quantify the effect of confinement degree on mean conformation of active polymers, we examine the root of mean-squared end-to-end distance $\sqrt{\langle R_e^2 \rangle} = \sqrt{\langle |\mathbf{r}_N - \mathbf{r}_1|^2 \rangle}$. Fig. 3 shows $\sqrt{\langle R_e^2 \rangle}$ against activity for different bending stiffness values and packing fractions. We first note that in free space, $\sqrt{\langle R_e^2 \rangle}$ has a weak dependence on active force for all degrees of flexibility. It decreases very little upon increase of f^a . Upon intro-

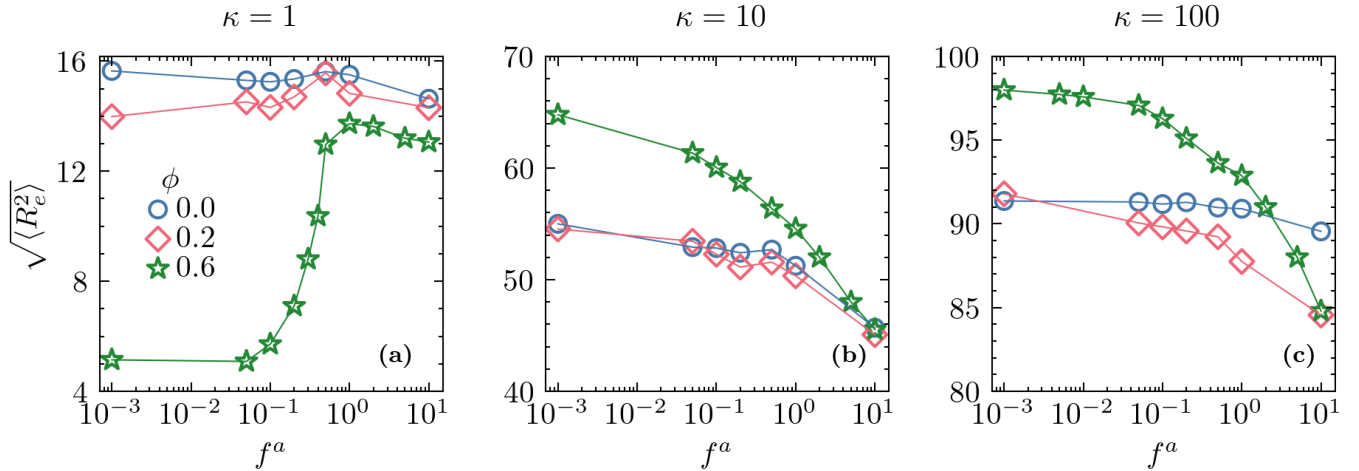


FIG. 3. The root of mean-squared end-to-end distance $\langle R_e \rangle$ versus active force f^a at packing fractions $\phi = 0, 0.2$ and 0.6 plotted for bending rigidity values (a) $\kappa = 1$, (b) $\kappa = 10$ and (c) $\kappa = 100$.

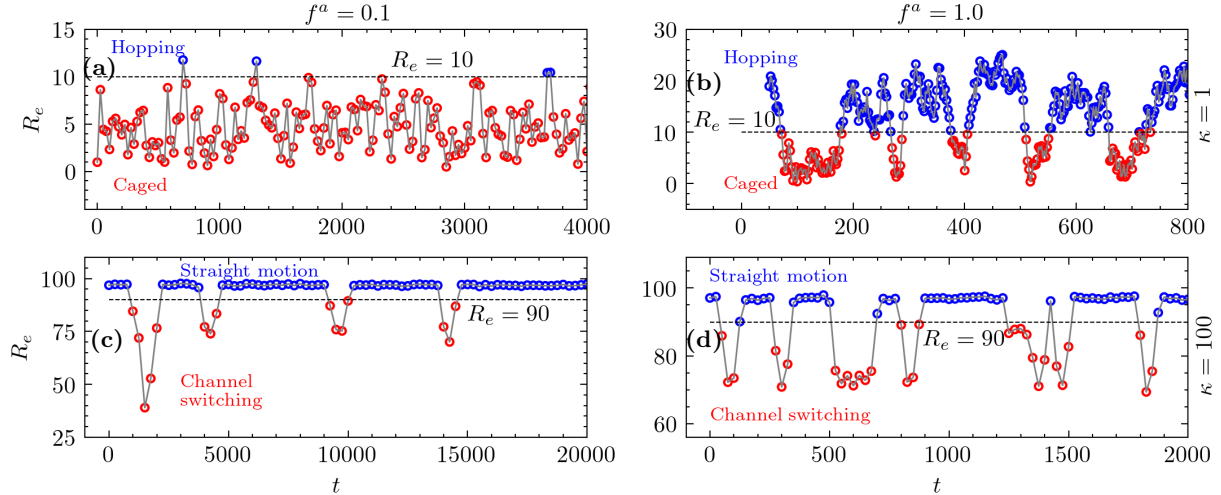


FIG. 4. End-to-end distance of a single polymer under strong confinement $\phi = 0.6$, with a) $\kappa = 1$ and $f^a = 0.1$, b) $\kappa = 1$ and $f^a = 1.0$, c) $\kappa = 100$ and $f^a = 0.1$ and d) $\kappa = 100$ and $f^a = 1.0$. The dashed lines show the threshold on R_e^* , above which chains are hopping or having straight motion depending on their stiffness. (a) and (b) show the characterization of hopping and caging events for flexible polymers. (c) and (d) show the characterization of straight motion through inter-obstacle channels and channel switching events for stiffer chains.

ducing periodic obstacles, for low density of obstacles at $\phi = 0.2$, $\sqrt{\langle R_e^2 \rangle}$ decreases only slightly for all κ values, the exact amount of which depends on the degree of activity and flexibility. However, for tight confinement at $\phi = 0.6$, we observe a remarkable change of $\sqrt{\langle R_e^2 \rangle}$ for all degrees of flexibility, albeit in contrasting trends for flexible and stiff polymers.

For Flexible chains with $\kappa = 1$, at $\phi = 0.6$, chains of low activity $f^a \leq 0.1$ have significantly smaller mean end-to-end distance than the free polymers with identical active force, whereas for $f^a > 0.1$ we observe a rather sharp increase of $\sqrt{\langle R_e^2 \rangle}$ reaching a maximum

at $f^a = 1$ beyond which its values becomes almost constant being only a little smaller than the $\sqrt{\langle R_e^2 \rangle}$ of free polymers. Visual inspection of movement of flexible polymers with low levels of activity through the obstacles, see Fig. 2 and video S10 in SM [24], reveals that in tight confinement, they remain localized within interobstacle pores, referred to as cages, most of the time and only occasionally unwind and hop to one of their adjacent cages. Figs. 4(a) and (b) depict temporal evolution of end-to-end distance of an individual active polymer with $f^a = 0.1$ and 1 . When a chain is caged its end-to-end distances is small, but while hopping it has a

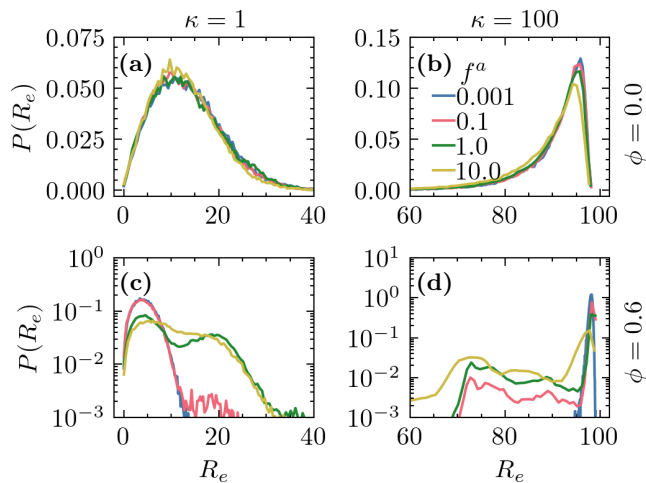


FIG. 5. The probability distribution function of end-to-end distance at different activity levels for polymers moving in free space *i.e.*, $\phi = 0$ a) $\kappa = 1$ and b) $\kappa = 100$ and $\phi = 0.0$ and for polymers under strong confinement with $\phi = 0.6$ c) $\kappa = 1$ and d) $\kappa = 100$.

more extended conformation and its end-to-end distance is larger. We note that with increasing the activity level, the chains become enabled to escape their cages and travel a short distance to one of their four neighboring cages, increasing frequency of the hopping events. For instance, at $f^a = 1$ the chains hop more frequently from one cage to another, compare Figs. 4(a) and (b) and see video S11 in SM [24]. As a result of their increased hopping frequency, the average end-to-end distance of highly active chains increases.

As mentioned earlier, we observe a remarkably different trend for $\sqrt{\langle R_e^2 \rangle}$ of stiffer chains. As presented in Figs. 3 (b) and (c), for $\kappa = 10$ and 100, tight confinement results in a larger end-to-end distance at all levels of activity. However, degree of extension of polymers decreases with increase of activity level. At packing fraction of $\phi = 0.6$, semiflexible active chains with $\ell_p^0 = 20$ and 200 ($\kappa = 10$ and 100) tend to travel through inter-obstacle horizontal/vertical channels as their persistence lengths are much larger than the channel width $\xi = 2.5$. Nonetheless, active polymers occasionally bend and turn into an adjacent perpendicular channel, see Fig. 2 and video S9 in SM [24]. We refer to this behavior as channel switching. During a channel switching event, a polymer bends and its end-to-end distance decreases, see Fig. 4(c) and (d) showing end-to-end distance of a stiff active polymer with $\kappa = 100$ for $f^a = 0.1$ and 1 versus time. The folding of backbone of a polymer during a channel switching event results in higher bending energy compared to straight conformation, which is more costly for stiffer chains. However, sufficiently large active forces can overcome the bending energy barriers for a channel switching event. As a result, upon increase of f^a , stiff chains

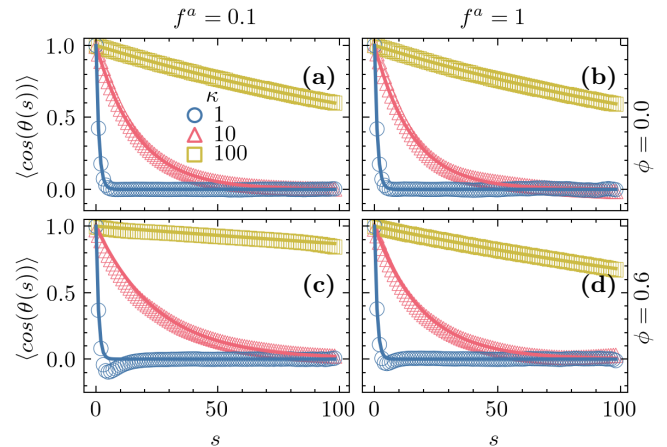


FIG. 6. The bond-bond correlation functions $\cos\theta(s)$ for various bending rigidity κ values for free chains with active force a) $f^a = 0.1$ and b) $f^a = 1$ and at packing fraction of $\phi = 0.6$ for active force c) $f^a = 0.1$ and d) $f^a = 1$. The solid lines show the exponential fits to the data in the range $1 \leq \langle \cos(\theta(s)) \rangle \leq e^{-1}$.

switch their channels more frequently, see Fig. 4(c) and (d) explaining the decline of $\sqrt{\langle R_e^2 \rangle}$ of confined polymers with active force. Increase of the end-to-end distance in tight confinement is more pronounced for stiffer chains, for which channel switching events occur less frequently due to the higher costs of bending.

To quantify our observation of different modes of chain conformation resulting from interaction with obstacles, we extract the probability distribution function (PDF) of the end-to-end distance $P(R_e)$ presented in Fig. 5. For active chains in free space, see Fig. 5 (a) and (b), $P(R_e)$ displays only a single peak, the value of which is primarily determined by the stiffness of the polymers and weakly depends on the active force. In contrast, under strong confinement at $\phi = 0.6$, the PDFs of end-to-end distance becomes broader. At sufficiently high activity levels, we distinguish two distinct peaks in the PDFs for both flexible and stiff polymers, verifying two different conformational modes of active chains confined within periodic channels. For active flexible chains with $f^a \geq 0.1$, the two peaks correspond to conformations in caged and hopping modes, respectively. For stiff chains with $f^a \geq 0.1$ the sharp peaks at large R_e correspond to elongated polymer conformations traveling straight within the inter-obstacle channels whereas the broader peaks at smaller R_e represent the chain conformations in channel switching mode.

B. Effect of periodic confinement on persistence length

Having investigated the effects of periodic confinement on the end-to-end distance statistical features, next we look into its effect on the shape of polymers. To this end,

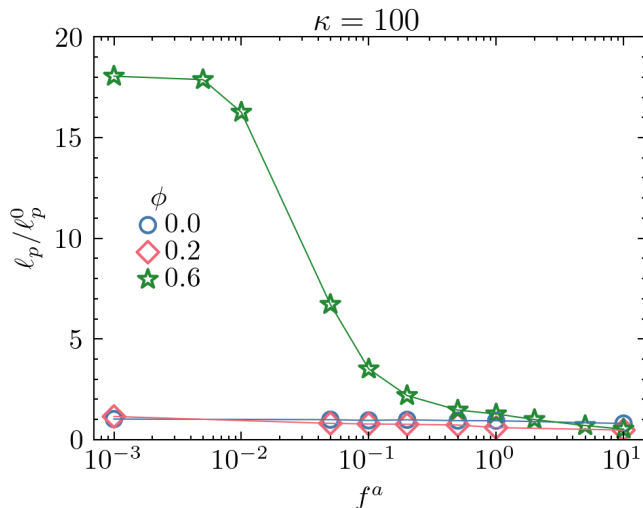


FIG. 7. The effective persistence length normalized by the persistence length of passive chains in free surface ℓ_p/ℓ_p^0 against active force f^a for various packing fraction ϕ and bending rigidity of $\kappa = 100$.

we compute the bond-bond correlation function defined as $\langle \cos(\theta(s)) \rangle$, where $\theta(s)$ is the angle between two bond vectors with a curvilinear distance s . Fig. 6 shows the bond-bond correlation functions for different activity levels and bending rigidity values in free space and under strong confinement at $\phi = 0.6$.

For flexible polymers ($\kappa = 1$), regardless of the degree of confinement and activity, bond-bond correlations drop to zero at short curvilinear distances ($s < 5$). The only notable effect at strong confinement ($\phi = 0.6$) is the appearance of a weak negative dip in $\langle \cos(\theta(s)) \rangle$ before decaying to zero reflecting the more shrunken conformation of polymers in caged state relative to the freely moving polymers.

For stiff chains ($\kappa = 100$), strong confinement visibly leads to a slower decay of bond-bond correlation functions with curvilinear distance s , see Figs. 6(c) and (d), the pace of which depends on the active force. To quantify this effect, we obtain the effective persistence lengths ℓ_p with the following protocol. First, we define s_e as the curvilinear distance at which the correlation becomes equal to e^{-1} , *i.e.*, $\langle \cos(\theta(s_e)) \rangle \leq e^{-1}$. For the cases where the correlations never reach e^{-1} , we choose $s_e = N - 1$. We then fit the bond correlation data in the range $0 \leq s \leq s_e$ by an exponential function $\langle \cos(\theta(s)) \rangle = \exp(-s/\ell_p)$ and evaluate the persistence length. Fig. 7 shows the effective persistence length ℓ_p of stiff polymers with $\kappa = 100$ normalized by the bare persistence length of passive free polymers, *i.e.*, $\ell_p^0 = 2\kappa$ versus active force at three packing fractions. At $\phi = 0.0$ and $\phi = 0.2$, we observe no significant changes of ℓ_p with activity level. However, for the stronger confinement at $\phi = 0.6$, marked changes in the effective persistence length emerge. As discussed earlier, the transport

of stiff active chains within a dense periodic array of obstacles at $\phi = 0.6$ consists of a sequence of straight paths within horizontal or vertical channels and channel switching events, the frequency of which increases with active force. A slightly active stiff polymer with $f^a = 10^{-3}$ and $\kappa = 100$ almost always travels in the same channel, and barely switches to another one. Thus its backbone stays straight most of the time resulting effectively in larger persistence length (almost 20 times larger than the chains moving in free space). However, by increasing active force and thereby frequency of channel switching events, polymers bend more often. Hence, their effective persistence length decreases.

IV. FLEXIBILITY-DEPENDENT MODES OF TRANSPORT

In the previous section, we demonstrated that strong periodic confinement $\phi = 0.6$ affects conformation of flexible and stiff active polymers differently. Increased confinement promotes greater contraction of flexible polymers, whereas it results in more elongated polymer conformations for stiffer polymers. This difference leads to distinct modes of transport for flexible and stiff polymers within tight inter-obstacle pores. The motion of active flexible polymers in the periodic lattice of obstacles consists of a sequence of caging and hopping events, whereas the motion of stiff chains consists of travelling straight in the tight channels and occasional bending of polymers to switch to an adjacent perpendicular channel. In this section, we examine the dynamics of individual active polymers as they navigate through the interobstacle space by obtaining the distribution of the duration of caging events and the time span of the directed motion in channels.

We first focus on flexible active polymers with $\kappa = 1$. To be able to quantify the duration of caging events, we define a caged state when the end-to-end distance of a polymer is smaller than a threshold value R^* , which we choose to be the diameter of inter-obstacle pore d_{cage} , see Fig. 4 (a) and (b). For tight confinement with $\xi = 2.5$, we have $d_{cage} \approx 10$ and time intervals with $R_e < R^*$ ($R_e > R^*$) characterize caging (hopping) events, see Figs. 4 (a) and (b). Fig. 8 (a) shows the distribution of caging time τ_{cage} for different active forces. We notice that the caging times span several orders of magnitude. The maximum caging time observed within our simulation time depends on the activity level and is largest for the lowest active force. We do not recognize a power law behavior for distribution of caging time. From these distribution functions, we extract the mean duration of caging events $\langle \tau_{cage} \rangle$ as functions of active force as presented in Fig. 8(b). We find that the mean caging time is roughly constant up to $f^a = 0.2$ and afterwards it decreases with f^a .

For stiffer chains with $\kappa = 100$ in tight confinement, interactions of a polymer with periodic array of obsta-

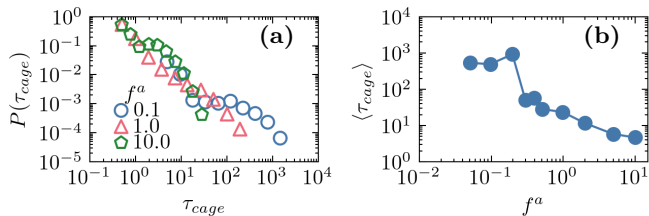


FIG. 8. a) The probability distribution function of caging time τ_{cage} for flexible chains with $\kappa = 1$ in tight confinement with $\phi = 0.6$ and for different activities. b) The mean values of $\langle \tau_{cage} \rangle$.

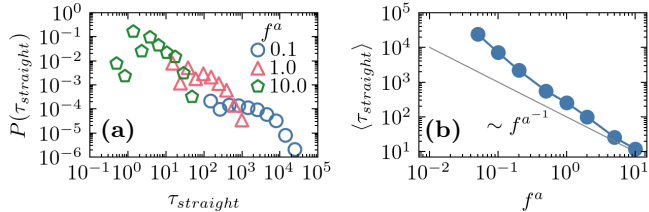


FIG. 9. a) The probability distribution function of straight traveling time $\tau_{straight}$ for polymers with $\kappa = 100$ in tight confinement with $\phi = 0.6$ and for different activities. b) The mean values of $\langle \tau_{straight} \rangle$.

cles result in a sequence of directed motion through channels and channel switching events. Similar to the case of caging-hopping events, the distinction between unidirectional traveling and channel switching states can be made by monitoring the instantaneous value of R_e of individual polymers. While travelling in a channel, the R_e is comparable to the chain length N . However, during a channel switching event where a polymer bends, its R_e decreases, see Fig. 4 (c) and (d). To find the threshold, we refer to $P(R_e)$ presented in Fig. 5(d), where the probability distribution functions have a sharp peak at large R_e corresponding to travelling within inter-obstacle channels. Among different activities, the sharp peak of $f^a = 10$ is broader and includes a minimum value of $R_e \approx 90$. We therefore set the channel switching condition as $R_e \leq 90$ and find the time duration of straight travel in channels $\tau_{straight}$ as the time interval for which $R_e > 90$. Fig. 4 (c) and (d) demonstrate how we distinguish between events of channel switching and straight motion for stiff chains with $\kappa = 100$. In Fig. 9 (a), we present the PDF of $\tau_{straight}$ for stiff chains with $\kappa = 100$ at $\phi = 0.6$. The typical time span of straight motion through the channels depends strongly on the activity level. The extracted mean values $\langle \tau_{straight} \rangle$ are presented in Fig. 9(b), which decrease with active force, scaling as $1/f^a$ for $f^a \gtrsim 0.1$.

This emergence of two different scaling regimes in $\langle \tau_{straight} \rangle$ against active force can be understood in terms of competition between two time scales. The first one is the timescale of advection by active force for the frontal

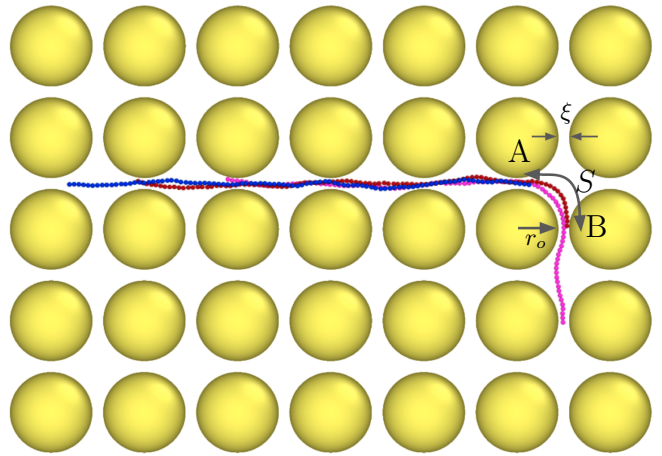


FIG. 10. Snapshots of a chain with $\kappa = 100$ and $f^a = 1.0$ traveling in a periodic medium with $\phi = 0.6$. The polymer enters the crossing area at point A. It actively changes the backbone orientation of its head segment toward point B. The chain leaves the crossing in a new channel.

segment of active polar polymer and the second one is the timescale of the relaxation of bending fluctuations. A channel switching event involves traveling of a minimal segment of length S of the polymer. S represents the frontal segment of a polymer that is involved during the turning of the polymer as shown in Fig. 10 when the head monomer moves from point A to B. It can be approximated as $S \approx \pi/2(r_o + \xi/2)$. The time required for the head bead to travel a curvilinear distance S is simply the advection time by active force $\tau_a^{adv} = S/f^a$. On the other hand the timescale for passive relaxation of bending fluctuation of a segment of curvilinear length S of a semiflexible polymer, according to the wormlike chain model (WLC), is given by $\tau_{bend} = S^4/(2\kappa)$ [25]. A channel switching event entails that the $\tau_a^{adv} < \tau_{bend}$ such that by increasing activity, a chain can switch its channel before the bending fluctuations on the scale of S can relax. A quick calculation using $\xi = 2.5$ for $\phi = 0.6$ and $\kappa = 100$ shows that $S \approx 15$ and the threshold activity (where $\tau_a^{adv} = \tau_{bend}$) is $f^a = 0.06$. As can be seen for $f^a > 0.1$, $\langle \tau_{straight} \rangle$ enters the $1/f^a$ scaling regime.

V. DYNAMICAL PROPERTIES

Having discussed the effects of periodic confinement on conformational properties of active polymers and their modes of transport under tight confinement, we subsequently investigate the effects of periodic confinement on their dynamical properties.

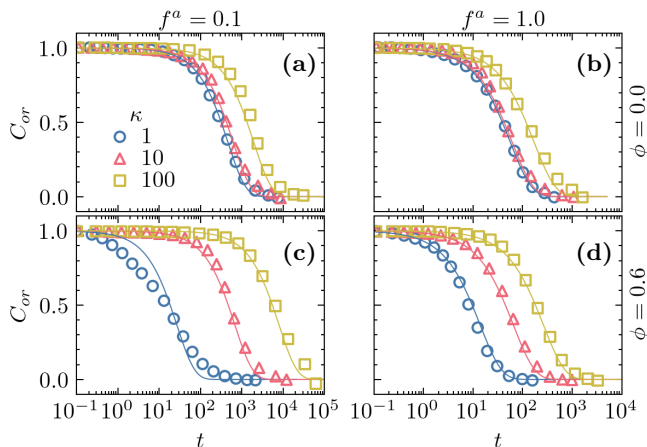


FIG. 11. The TACF of end-to-end unit vector, C_{or} , for different bending rigidity values $\kappa = 1, 10$ and 100 for free chains with active force a) $f^a = 0.1$ and b) $f^a = 1$ and in periodic lattice of obstacles with packing fraction of $\phi = 0.6$ for active force c) $f^a = 0.1$ and d) $f^a = 1$. The lines depict exponential fits to the data for the time interval where $1 \leq C_e(t) \leq e^{-1}$.

A. Orientational dynamics

We start by examining the effects of periodic confinement on orientational dynamics of active polymers. Since a tangentially-driven polymer is polar (head-tail asymmetry), we define the end-to-end vector as $\mathbf{R}_e(t) = \mathbf{r}_N(t) - \mathbf{r}_1(t)$. Thus, we characterize polymers orientational dynamics by the time auto-correlation function (TACF) of their end-to-end unit vector,

$$C_{or}(t) = \langle \hat{\mathbf{R}}_e(0) \cdot \hat{\mathbf{R}}_e(t) \rangle. \quad (2)$$

In Fig. 11, we present the orientational TACFs of active polymers in free space and in tight confinement $\phi = 0.6$ as functions of lag time for different bending rigidity values and at two active forces $f^a = 0.1$ and 1.0 . In free space, for a given active force upon increase of bending stiffness, the orientational correlation functions decay slower, whereas by increasing active force, they decay faster, which is in agreement with prior reports for flexible active polymers [26–28]. When introducing obstacles with $\phi = 0.6$, the periodic confinement can accelerate or slow down orientational dynamics depending on the bending stiffness and activity level. At $f^a = 0.1$ and $\phi = 0.6$, we observe a much slower decay of the orientational TACF for stiff chains with $\kappa = 100$ compared to the freely moving chains with the same active force and bending stiffness, whereas the orientational dynamics of flexible polymers becomes accelerated. At higher active force of $f^a = 1.0$, the orientational dynamics of flexible active polymers in tight periodic confinement is again faster than those of chains in free space. On the other hand, for very stiff polymers with $\kappa = 100$, the orientational dynamics of active polymers in free space and tight periodic confinement become similar.

In order to quantify the effect of periodic confinement on the decay of orientational dynamics, we define a characteristic reorientational relaxation time τ_r with the following protocol. First, we define t_e as the shortest lag time at which the normalized correlation becomes less than e^{-1} , *i.e.*, $C_{or} \leq e^{-1}$. We then fit the data in the range $0 \leq t \leq t_e$ with an exponential function $C_{or} = \exp(-t/\tau_r)$ from which we determine the reorientational relaxation time τ_r . The extracted orientational relaxation times as functions of active force are shown with open symbols in Fig. 12 for different values of bending rigidity κ and ϕ . First, we focus on the flexible polymer limit with $\kappa = 1$ shown in Fig. 12(a). For free chains and those in moderate confinement with $\phi = 0.2$, τ_e scales as $1/f^a$ for $f^a \geq 0.1$, similar to the findings of prior research on isolated active polymers [26, 28]. However, in tight confinement $\phi = 0.6$, chains with low and moderate active forces ($f^a \leq 1$) have a much faster orientational dynamics and thus shorter relaxation times as a result of being caged between neighbouring obstacles. However, at higher activities $f^a \geq 2$, where the chains more frequently hop to adjacent cages, the orientational relaxation time becomes equal to that of freely moving active polymers.

For intermediate stiffness with $\kappa = 10$, the orientational relaxation times are shown in Fig. 12(b). For $f^a \geq 0.05$, τ_r perfectly follows the $1/f^a$ scaling behaviour similar to isolated active flexible polymers [26, 28], suggesting the dominance of activity over confinement in this case. For stiff chains with $\kappa = 100$, free chains and those in moderate confinement with $\phi = 0.2$ have identical relaxation times following the $1/f^a$ scaling for $f^a \geq 0.05$. In contrast, at $\phi = 0.6$ we observe two different regimes. At higher activities ($f^a \geq 0.2$) the orientational relaxation times of strongly confined polymers are of the same order of magnitude as τ_r of isolated chains, while less active polymers have notably larger τ_r . These results can be understood in view of confinement degree defined as the ratio of intrinsic persistence length of a polymer ℓ_p^0 to the channel width of the medium ξ . For strong confinement ($2\kappa/\xi = 200/2.5 \gg 1$), the polymer is forced to keep travelling within one channel in a rather elongated conformation, see Fig. 2. Hence, orientational dynamics is very slow as it entails overcoming the bending energy of very stiff polymers for switching to another channel. At sufficiently high activities, the active force can overcome the bending energy barriers for channel switching and the $1/f^a$ scaling behavior reemerges. However, less active chain can barely switch their channels, resulting in orientational relaxation times almost one order of magnitude larger than that of isolated chains at $f^a = 0.05$.

B. Translational dynamics

Next we explore the translational dynamics of active polymers under periodic confinement by computing the mean squared displacement (MSD) of the center of

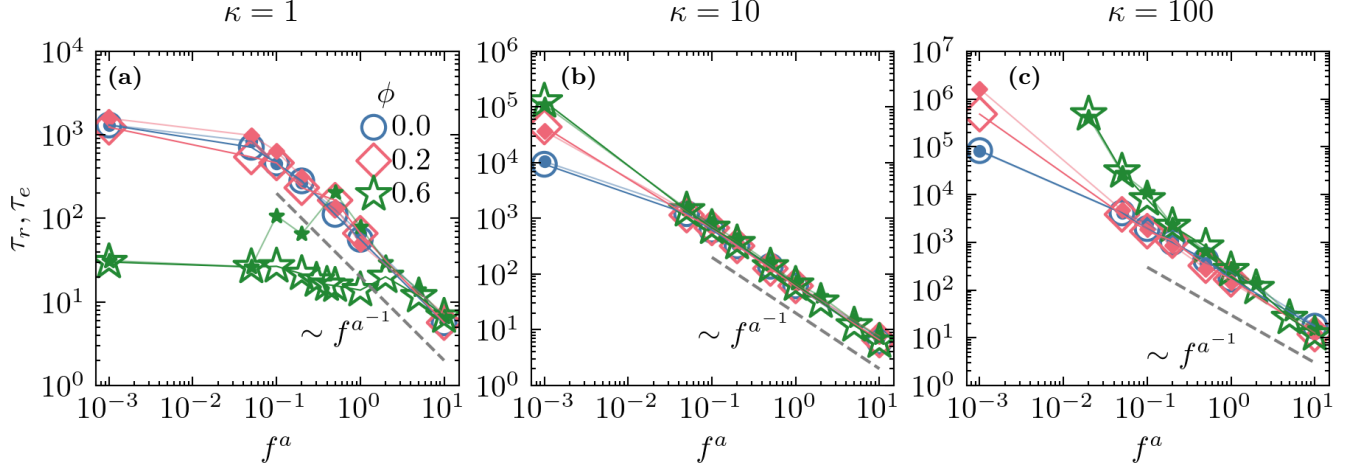


FIG. 12. The end-to-end unit vector relaxation time τ_r (open symbols) versus active force f^a for various packing fraction ϕ and bending rigidity of (a) $\kappa = 1$, (b) $\kappa = 10$ and (c) $\kappa = 100$. The closed symbols show the relaxation time of the end-to-end vector τ_e for $\kappa = 10$ and $\kappa = 100$, respectively.

mass. Defining the position of the center of mass at any time as $\mathbf{R}_{cm}(t) = \frac{1}{N} \sum \mathbf{r}_i(t)$, the MSD is computed as $\langle \Delta \mathbf{R}_{cm}^2(t) \rangle = \langle |\mathbf{R}_{cm}(t) - \mathbf{R}_{cm}(0)|^2 \rangle$. Fig. 13 presents MSD curves as functions of lag time in free space and strong confinement $\phi = 0.6$ for different bending rigidity values and at two active forces $f^a = 0.1$ and 1. Regardless of defining parameters of chains and their surrounding media (f^a , κ and ϕ), in all the MSD curves, we observe three distinct scaling regimes. At very short lag times, where the MSD values are initially proportional to t , the fluctuations of random forces are more dominant over active force and interactions with obstacles, hence the translational motion is governed by thermal diffusion and the MSD has the form $\langle \Delta \mathbf{R}_{cm}^2 \rangle = 4D_{Passive}^{Free} t$, where

$D_{Passive}^{Free} = D_0/N = 0.01$ is the diffusion coefficient of a passive chain consisted of $N = 100$ monomers moving in free space. At longer lag times active forces and interactions with obstacles come into play and the chains enter an intermediate regime.

At intermediate timescales, for chains in free space, this motion is ballistic $\langle \Delta \mathbf{R}_{cm}^2 \rangle \sim t^2$ and is associated with the total active force on the center of mass of polymers [26, 28, 29]. At this range of lag times, the motion of the center of mass of freely moving active polymers can roughly be interpreted as moving straight with a constant speed in the direction of total active force. The net active force on center of mass for a tangentially-driven active polymer is given by $\mathbf{F}^a(t) = \sum_{i=1}^N \mathbf{f}_i^a(t) = f^a \mathbf{R}_e(t)/\ell$, being parallel to the end-to-end vector. Therefore, we expect that the timescale for departure from straight motion is set by τ_r , *i.e.* the relaxation time of the end-to-end vector TACF. The observed ballistic regime at intermediate timescales remains intact even in the presence of obstacles for all the cases apart from low activity flexible chains with active force $f^a = 0.1$ and under tight confinement $\phi = 0.6$, which exhibit a sub-diffusive behaviour with an MSD growing as $t^{0.4}$, see Fig. 13(c). The observed subdiffusive regime is a consequence of transient caging dynamics of flexible active polymers, which are trapped in the inter-obstacle pores and from time to time hop to one of their adjacent cages.

At longer lag times when $t \gg \tau_r$, after active chains have lost the memory of their initial end-to-end vector direction, a final diffusive regime with enhanced long-time diffusion coefficient D_L emerges, *i.e.* $\langle \Delta \mathbf{R}_{cm}^2(t \gg \tau_e) \rangle = 4D_L t$. The D_L values, extracted from linear fits of the MSD curves at large lag times, against activity are presented in Fig. 14 for $\phi = 0, 0.2$ and 0.6 and different κ values. For $\phi = 0.6$, for $\kappa = 1$ and 100 and $f^a \leq 0.05$, we did not observe a final diffusive regime within our simulation run time, therefore we cannot report D_L

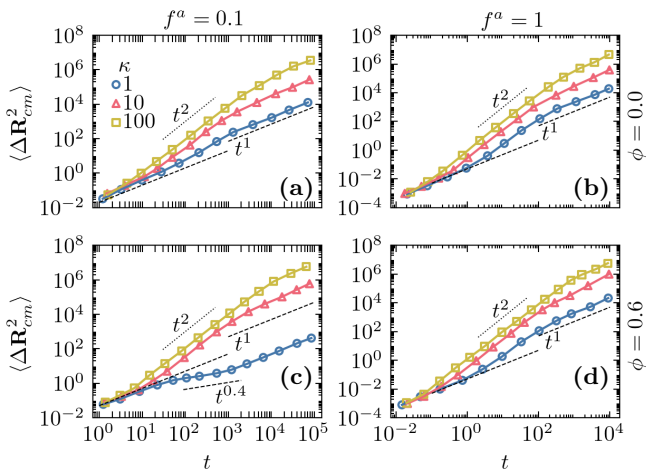


FIG. 13. The MSD $\Delta \mathbf{R}_{cm}^2$ for various bending rigidity values for free chains with active force a) $f^a = 0.1$ and b) $f^a = 1$ and at packing fraction of $\phi = 0.6$ for active force c) $f^a = 0.1$ and d) $f^a = 1$.

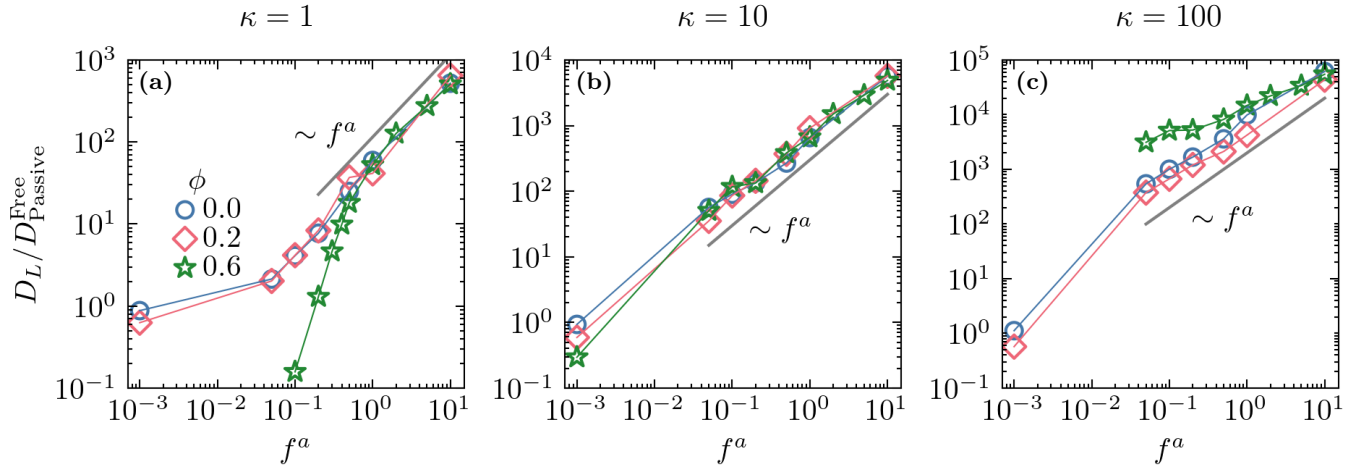


FIG. 14. The normalized long time diffusion coefficient D_L/D_{Passive} versus active force f^a for packing fractions $\phi = 0, 0.2$ and 0.6 and bending rigidity of (a) $\kappa = 1$, (b) $\kappa = 10$ and (c) $\kappa = 100$. In panel (a), for $\phi = 0.6$, the chains with $f^a = 0.001$ and $f^a = 0.05$ never entered the final diffusive regime within our simulation time, therefore we cannot report D_L values for them.

values for these cases. For active chains in free space with $f^a > 0.05$, the D_L increases linearly with active force in agreement with theoretical predictions [27] and previous simulations [26, 28].

A moderate periodic confinement $\phi = 0.2$ does not significantly affect the long-time diffusion coefficient for all values κ and the linear scaling with f^a remains intact. However, effect of tight confinement on D_L very much depends on the bending rigidity. Interestingly, the D_L of active chains with moderate bending stiffness $\kappa = 10$, see Fig. 14(b) is not much affected by strong confinement and it increases linearly with activity. At $\phi = 0.6$, the D_L of flexible active polymers $\kappa = 1$ for active forces $f^a < 0.5$ is lower than those of free chains, whereas D_L of very stiff chains $\kappa = 100$ for active forces $0.05 \leq f^a \leq 0.5$ is remarkably enhanced. These contrasting trends reflect the different modes of transport for flexible and stiff polymers. For flexible polymers, caging of polymers with low active forces slows down the diffusion as diffusion only occurs via occasional hopping events. In contrast, for stiff active polymers, the persistent unidirectional transport in the inter-obstacle channels helps them to diffuse through larger distances, thereby enhancing diffusion. Nonetheless, at sufficiently high activity levels, the long-time diffusion coefficients under tight confinement approach the D_L of active polymers in free space, regardless of their degree of flexibility.

C. Analytical calculations of center of mass dynamics

To rationalize the observed trends for the long-time diffusion coefficient of the center of mass, we derive the equation of center of mass velocity $\mathbf{V}_{\text{cm}}(t)$ explicitly. By summing over all the monomers velocities described by

Eq. (1), we obtain:

$$\gamma \mathbf{V}_{\text{cm}} = \frac{1}{N} (\mathbf{F}^a(t) + \mathbf{F}^r(t) + \mathbf{F}^o(t)), \quad (3)$$

where $\mathbf{F}^a = \sum_{i=1}^N \mathbf{f}_i^a(t)$ is the total active force, $\mathbf{F}^r = \sum_{i=1}^N \mathbf{f}_i^r(t)$ is the sum of all the random forces with a zero mean and $\langle \mathbf{F}^r(t) \cdot \mathbf{F}^r(t') \rangle = 4ND_0\gamma^2\delta(t-t')$ and $\mathbf{F}^o(t) = \sum_{i=1}^N \nabla U_{\text{excl}}(\mathbf{r}_i)$ is the total force resulting from interactions with obstacles. As previously mentioned, for a tangentially driven polymer the total active force is proportional to end-to-end vector $\mathbf{F}^a(t) = f^a \mathbf{R}_e(t)/\ell$.

In order to obtain the long-time diffusion, we need to compute the TACF of center of mass velocity. Taking into account that correlations of other forces with the total random force vanish, the TACF of the center of mass velocity is given by

$$\begin{aligned} C_v(t) &= \langle \mathbf{V}_{\text{cm}}(t) \cdot \mathbf{V}_{\text{cm}}(0) \rangle \\ &= \left(\frac{f^a}{N\ell\gamma} \right)^2 \langle \mathbf{R}_e(t) \cdot \mathbf{R}_e(0) \rangle \\ &\quad + \frac{f^a}{N\ell\gamma} [\langle \mathbf{R}_e(t) \cdot \mathbf{F}^o(0) \rangle + \langle \mathbf{F}^o(t) \cdot \mathbf{R}_e(0) \rangle] \\ &\quad + \frac{1}{N\gamma} \langle \mathbf{F}^o(t) \cdot \mathbf{F}^o(0) \rangle + \left(\frac{1}{N\gamma} \right)^2 \langle \mathbf{F}^r(t) \cdot \mathbf{F}^r(0) \rangle. \end{aligned} \quad (4)$$

We can simplify the above equation for semiflexible polymers with $\kappa \geq 10$ taking into account the following considerations. For $\kappa \geq 10$ and sufficiently large activities $f^a \geq 0.05$, the periodic confinement constrains active polymers with $\kappa \geq 10$ to move in the inter-obstacle channels, so the frequency of collisions is low and interactions with obstacles are somewhat random. Hence, we argue that the contributions from correlations of end-to-end vector and collisional forces, *i.e.* the third line of Eq. (4), are negligible. We emphasize that even though

we have neglected these contributions, the effects of collisions with obstacles are reflected in the dynamics of the end-to-end vector. Collision events change the mean end-to-end distance, see Fig. 3 as well as orientational dynamics, see section V A. Especially, increasing the degree of confinement ($2\kappa/\xi$) significantly increases orientational relaxation time for $\kappa = 100$ and moderate active forces, see Fig. 12(c).

Assuming that the fluctuations of end-to-end distance are negligible, justified for stiff active polymers, see Fig. 5 (b) and (d), and the TACF of end-to-end vector decays exponentially, we can approximate it as

$$\langle \mathbf{R}_e(t) \cdot \mathbf{R}_e(0) \rangle = \langle \mathbf{R}_e(t)^2 \rangle e^{-t/\tau_e} \quad (5)$$

where the decay time τ_e depends on activity, bending stiffness and packing fraction. We have also presented τ_e as a function of active force for different values of κ and ϕ in Fig. 12 as closed symbols. For $\kappa \geq 10$ τ_e and τ_r (open symbols) values are in good agreement. In contrast for flexible polymers at $\phi = 0.6$, where the polymers shrink in cages and extend during hopping τ_e and τ_r are different at intermediate active forces. Hence, our proposed approximation for them are not valid.

Taking into account the above considerations, we obtain the the following approximation for TACF of \mathbf{V}_{cm} of semiflexible polymers:

$$C_v(t > 0) \approx \frac{f^{a2}}{N^2 \ell^2 \gamma^2} \langle R_e^2 \rangle e^{-t/\tau_e} + \frac{1}{N\gamma} \langle \mathbf{F}^o(t) \cdot \mathbf{F}^o(0) \rangle + \left(\frac{1}{N\gamma}\right)^2 \langle \mathbf{F}^r(t) \cdot \mathbf{F}^r(0) \rangle. \quad (6)$$

Integrating this approximate C_v , we can obtain the long time diffusion coefficient as $D_L = \frac{1}{2} \int_0^\infty dt C_v(t)$. The terms in the second line of Eq. (6) includes contributions from TACFs of collisional and random forces, which do not depend on the active force. Hence their contributions to the integral can be represented as a packing fraction and bending stiffness dependent diffusion coefficient of a passive polymer $D_{\text{Passive}}^{\phi, \kappa}$. Consequently, D_L can be approximated as

$$D_L \approx D_{\text{Passive}}^{\phi, \kappa} + \frac{f^{a2} \langle R_e^2 \rangle \tau_e}{2N^2 \ell^2 \gamma^2}. \quad (7)$$

Passive stiff chains in high packing fraction media are confined to travel in inter-obstacle channels. Therefore their motion is effectively one dimensional with a diffusion coefficient of $D_{\text{Passive}}^{\text{Free}}/2$ [30]. By decreasing the degree of confinement the passive diffusion coefficient gradually increases until the D_L of free chains is recovered. We calculate the predictions of Eq. (7) using $\langle R_e^2 \rangle$ and τ_e from simulations. Comparison of D_L extracted from MSD curves with results of Eq (7) for semiflexible polymers, presented in Fig. 15, show good agreement.

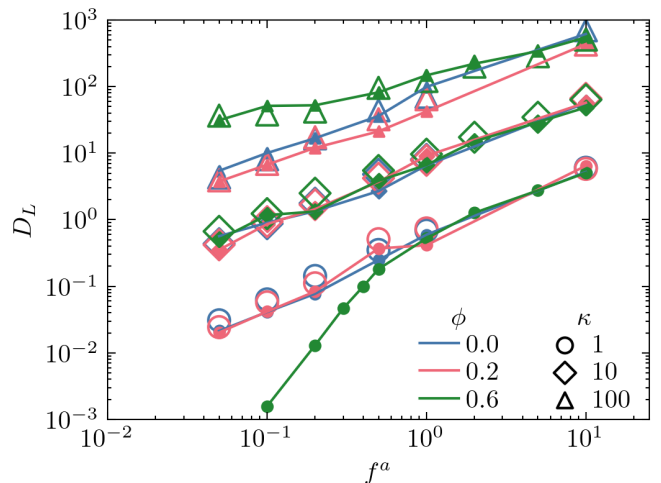


FIG. 15. Long-time diffusion coefficient D_L versus active force f^a for different packing fraction for semiflexible polymers of bending stiffness $\kappa = 1, 10$ and 100 . The closed symbols (with the lines as guides) show D_L values extracted from MSD curves. The open symbols show the results of eq. (7). For the case of $\kappa = 1$ and $\phi = 0.6$ the results of Eq. (7) are not presented as our assumptions are not valid in this case.

VI. CONCLUSION AND OUTLOOK

We have computationally studied the effects of periodic confinement, created by a square lattice of circular obstacles, on conformational and dynamical properties of semiflexible tangentially driven active polymers. We considered two packing fractions of obstacles, $\phi = 0.2$ and 0.6 . We find that effects of periodic confinement become significant only at the higher packing fraction $\phi = 0.6$ and its impact on conformation and dynamics strongly depends on the degree of flexibility and the activity level. For flexible polymers, notable changes arise when polymer size becomes comparable to the pore size, whereas for semiflexible polymers confinement effects predominate when the persistence length is much larger than the pore size. Strong periodic confinement ($\phi = 0.6$) affects conformation of flexible and stiff active polymers in distinct ways.

Flexible polymers in tight confinement become predominantly localized inside the interobstacle cages, resulting in shrunken conformations. However, active polymers occasionally succeed to hop from one cage to another via activity-induced conformational fluctuations enabling them to pass through the narrow channels in elongated conformations. This localization phenomenon is similar to what is found for transport of active polymers in disordered media [9]. Upon increase of active force, the time spent in cages decreases and frequency of hopping events increases, leading to more extended polymer conformations and larger mean end-to-end distances. As a result, we observe a relatively sharp transition from

a localized conformation to extended conformation as a function of active force. At low activity levels the orientational relaxation time of active flexible polymers is two orders of magnitudes smaller as the caged polymers rattle quickly inside the confinement pores. The long-time diffusion coefficient of center of mass is also substantially reduced. On the contrary, at high active forces polymers frequently hop from one cage to another. Interestingly, both orientational relaxation time and the long-time diffusion coefficient of highly active polymers approach those in free space.

In the other limit, strong confinement suppresses transverse fluctuations of stiff semiflexible polymers and enables them to migrate ballistically in elongated conformations within inter-obstacle channels. As a result, at low activity levels, we observe a notable increase of orientational relaxation time which in turn leads to enhancement of long-time diffusion of center of mass due to enhancement of persistent motion. On the other hand, high active forces can overcome the energetic costs associated with bending and enable active polymers to fold more frequently and to switch from one channel to another. This in turn results in decrease of orientational relaxation time and increase of long-time diffusion of center of mass such that polymers at high active forces navigate in tightly confined periodic environment as quick as free active polymers.

It is worth mentioning that despite the different modes of transport for flexible and stiff active polymers under tight confinement, at sufficiently large activity levels, we observe a robust scaling for the orientational relaxation time with active force decreasing as $1/f^a$. Moreover, the mean end-to-end distance at high activities also approaches to that of free polymers regardless of degree of flexibility. We finally presented an analytical approach for the long-time diffusion coefficient of the center of the mass of stiffer polymers ($\kappa \geq 10$), using justified approx-

imations. Our theoretical estimate is in good agreement with the direct results of the simulations, providing insights into roles of orientational relaxation time and mean end-to-end distance on the long-time diffusion coefficient.

In summary, the general emerging pattern observed in the dynamics of active chains with varying degrees of flexibility is that the transport of highly active chains remains unaffected by the level of confinement. On the contrary, at low activity levels, flexibility degree of active polymers plays a critical role for their transport through ordered porous media. This study suggests an optimal degree of flexibility for migration of active deformable particles in tight periodic confinement. This study is only the first step in understanding the motion of semiflexible tangentially driven polymers in heterogeneous ordered media and it calls for further investigations on the role of chain length, type of periodic lattice and generalization to periodic and disordered three-dimensional media in the future.

VII. SUPPLEMENTARY MATERIAL

The supplementary material supports the results presented in the main text and contains movie files.

VIII. ACKNOWLEDGEMENT

We acknowledge A. Deblais and R. Sinaasapple for fruitful discussions. The computations were carried out on the Dutch National e-Infrastructure with the support of the SURF Cooperative. This work was part of the D-ITP consortium, a program of the Netherlands Organization for Scientific Research (NWO) that is funded by the Dutch Ministry of Education, Culture and Science (OCW).

-
- [1] C. Bechinger, R. Di Leonardo, H. Löwen, C. Reichhardt, G. Volpe, and G. Volpe, *Rev. Mod. Phys.* **88**, 045006 (2016).
 - [2] O. Chepizhko, E. G. Altmann, and F. Peruani, *Phys. Rev. Lett.* **110**, 238101 (2013).
 - [3] O. Chepizhko and F. Peruani, *Phys. Rev. Lett.* **111**, 160604 (2013).
 - [4] T. Bhattacharjee and S. S. Datta, “Bacterial hopping and trapping in porous media,” (2019).
 - [5] C. Reichhardt and C. O. Reichhardt, *Physical Review E* **90**, 012701 (2014).
 - [6] C. Reichhardt and C. O. Reichhardt, *Physical Review E* **97**, 052613 (2018).
 - [7] A. Morin, N. Desreumaux, J.-B. Caussin, and D. Bartolo, *Nature Physics* **13**, 63 (2017).
 - [8] E. Irani, Z. Mokhtari, and A. Zippelius, *Phys. Rev. Lett.* **128**, 144501 (2022).
 - [9] Z. Mokhtari and A. Zippelius, *Phys. Rev. Lett.* **123**, 028001 (2019).
 - [10] L. Theeyancheri, S. Chaki, T. Bhattacharjee, and R. Chakrabarti, *The Journal of Chemical Physics* **159**, 014902 (2023).
 - [11] K. J. Modica, Y. Xi, and S. C. Takatori, *Frontiers in Physics* **10** (2022), 10.3389/fphy.2022.869175.
 - [12] D. M. van Roon, G. Volpe, M. M. Telo da Gama, and N. A. M. Araújo, *Soft Matter* **18**, 6899 (2022).
 - [13] R. Alonso-Matilla, B. Chakrabarti, and D. Saintillan, *Phys. Rev. Fluids* **4**, 043101 (2019).
 - [14] D. Shrestha, J. Ou, A. Rogers, A. Jereb, D. Okyere, J. Chen, and Y. Wang, *Colloids and Surfaces B: Biointerfaces* **222**, 113128 (2023).
 - [15] S. Pattanayak, R. Das, M. Kumar, and S. Mishra, *The European Physical Journal E* **42** (2019), 10.1140/epje/i2019-11826-7.
 - [16] A. Chamolly, T. Ishikawa, and E. Lauga, *New Journal of Physics* **19**, 115001 (2017).
 - [17] P. Chopra, D. Quint, A. Gopinathan, and B. Liu, *Phys. Rev. Fluids* **7**, L071101 (2022).

- [18] E. P. Ivanova, J. Hasan, H. K. Webb, V. K. Truong, G. S. Watson, J. A. Watson, V. A. Baulin, S. Pogodin, J. Y. Wang, M. J. Tobin, C. Lötbe, and R. J. Crawford, *Small* **8**, 2489 (2012), <https://onlinelibrary.wiley.com/doi/pdf/10.1002/sml.201200526>.
- [19] J. F. Schumacher, M. L. Carman, T. G. Estes, A. W. Feinberg, L. H. Wilson, M. E. Callow, J. A. Callow, J. A. Finlay, and A. B. Brennan, *Biofouling* **23**, 55 (2007).
- [20] T. Heeremans, A. Deblais, D. Bonn, and S. Woutersen, *Science Advances* **8**, eabj7918 (2022).
- [21] R. E. Isele-Holder, J. Elgeti, and G. Gompper, *Soft Matter* **11**, 7181 (2015).
- [22] J. D. Weeks, D. Chandler, and H. C. Andersen, *The Journal of Chemical Physics* **54**, 5237 (1971).
- [23] K. Binder, S. A. Egorov, A. Milchev, and A. Nikoubashman, *Journal of Physics: Materials* **3**, 032008 (2020).
- [24] “See supplemental material at url for sample videos and simulation parameters which includes ref.[...].”.
- [25] R. Everaers, F. Jülicher, A. Ajdari, and A. C. Maggs, *Phys. Rev. Lett.* **82**, 3717 (1999).
- [26] V. Bianco, E. Locatelli, and P. Magaretti, *Phys. Rev. Lett.* **121**, 217802 (2018).
- [27] C. A. Philipps, G. Gompper, and R. G. Winkler, *The Journal of Chemical Physics* **157**, 194904 (2022).
- [28] M. Fazelzadeh, E. Irani, Z. Mokhtari, and S. Jabbari-Farouji, *Phys. Rev. E* **108**, 024606 (2023).
- [29] R. G. Winkler and G. Gompper, *The Journal of Chemical Physics* **153**, 040901 (2020).
- [30] G. Nam, A. Johner, and N.-K. Lee, *The Journal of Chemical Physics* **133**, 044908 (2010).
- [31] J. A. Anderson, J. Glaser, and S. C. Glotzer, *Computational Materials Science* **173**, 109363 (2020).